doi:10.1093/brain/awr202 Brain 2011: 134; 2929–2947 | 2929

BRAIN
A JOURNAL OF NEUROLOGY

Interictal-like network activity and receptor expression in the epileptic human lateral amygdala

Stéphanie Graebenitz,[1,*] Olga Kedo,[1,2,*] Erwin-Josef Speckmann,[1,3] Ali Gorji,[1] Heinz Panneck,[4] Volkmar Hans,[5] Nicola Palomero-Gallagher,[2] Axel Schleicher,[6] Karl Zilles[2,6] and Hans-Christian Pape[1,3]

1 Institute of Physiology I, Westfaelische Wilhelms-Universität Münster, D-48149 Münster, Germany
2 Institute of Neuroscience and Medicine, Research Centre Jülich, D-52425 Jülich, Germany
3 Institute for Experimental Epilepsy Research, Westfälische Wilhelms-Universität Münster, D-48149 Münster, Germany
4 Bethel Epilepsy Centre Bethel, Mara, D-33617 Bielefeld, Germany
5 Institute of Neuropathology, Bethel, D-33617 Bielefeld, Germany
6 C and O Vogt-Institute of Brain Research, Heinrich-Heine-University Düsseldorf, D-40225 Düsseldorf, Germany

*These authors contributed equally to this work.

Correspondence to: Hans-Christian Pape,
Institute of Physiology I, Robert-Koch Str. 27a,
D-48149 Münster, Germany
E-mail: papechris@ukmuenster.de

or: Karl Zilles,
Institute of Neuroscience and Medicine-2,
Research Center Jülich,
D-52425 Jülich, Germany
E-mail: k.zilles@fz-juelich.de

While the amygdala is considered to play a critical role in temporal lobe epilepsy, conclusions on underlying pathophysiological mechanisms have been derived largely from experimental animal studies. Therefore, the present study aimed to characterize synaptic network interactions, focusing on spontaneous interictal-like activity, and the expression profile of transmitter receptors in the human lateral amygdala in relation to temporal lobe epilepsy. Electrophysiological recordings, obtained intra-operatively *in vivo* in patients with medically intractable temporal lobe epilepsy, revealed the existence of interictal activity in amygdala and hippocampus. For *in vitro* analyses, slices were prepared from surgically resected specimens, and sections from individual specimens were used for electrophysiological recordings, receptor autoradiographic analyses and histological visualization of major amygdaloid nuclei for verification of recording sites. In the lateral amygdala, interictal-like activity appeared as spontaneous slow rhythmic field potentials at an average frequency of 0.39Hz, which occurred at different sites with various degrees of synchronization in 33.3% of the tested slices. Pharmacological blockade of glutamate α-amino-3-hydroxy-5-methyl-4-isoxazolepropionic acid receptors, but not *N*-methyl-D-aspartate receptors, abolished interictal-like activity, while the γ-aminobutyric acid A-type receptor antagonist bicuculline resulted in a dampening of activity, followed by highly synchronous patterns of slow rhythmic activity during washout. Receptor autoradiographic analysis revealed significantly higher α-amino-3-hydroxy-5-methyl-4-isoxazolepropionic acid, kainate, metabotropic glutamate type 2/3, muscarinic type 2 and adrenoceptor α_1 densities, whereas muscarinergic type 3 and serotonergic type 1A receptor densities were lower in the lateral amygdala from epileptic patients in comparison to autopsy controls. Concerning γ-aminobutyric acid A-type receptors, agonist binding was unaltered whereas antagonist binding sites were downregulated in the epileptic lateral amygdala, suggesting an altered high/low-affinity state ratio and concomitant reduced pool of total γ-aminobutyric acid A-type receptors. Together these data indicate an abnormal pattern of receptor densities and synaptic function in the lateral nucleus of the amygdala in epileptic patients,

Received March 30, 2011. Revised May 20, 2011. Accepted June 17, 2011. Advance Access publication September 5, 2011

involving critical alterations in glutamate and γ-aminobutyric acid receptors, which may give rise to domains of spontaneous interictal discharges contributing to seizure activity in the amygdala.

Keywords: lateral amygdala; human temporal lobe epilepsy; field potentials; transmitter receptors; intra-operative recording

Abbreviations: AMPA = α-amino-3-hydroxy-5-methyl-4-isoxazolepropionic acid; APV = DL-2-amino-5-phosphono-valerate; CNQX = 6-cyano-7-nitro-quinoxaline-2,3-dione; CSF = cerebrospinal fluid; EEG = electroencephalogram; GABA = aminobutyric acid; MRI = magnetic resonance imaging; NMDA = *N*-methyl-D-aspartate; ns = not significant

Introduction

The amygdala is well-known for its implication in temporal lobe epilepsy, the most common adult type of refractory focal epilepsy (Engel *et al*., 2007). It is also considered a key structure for emotional modulation of behaviour and memory (LeDoux, 2000) and may be linked to the experience of fear and anxiety reported by patients before or in between the occurrence of temporolimbic seizures (Gloor, 1992; Cendes *et al*., 1994; Biraben *et al*., 2001). Depth electrode explorations in patients with refractory temporal lobe epilepsy revealed an involvement of the amygdala in 32% of focal seizures and in 91% of regional seizures (Quesney, 1986). Neuronal loss and gliosis occur in the amygdala also in the absence of hippocampal sclerosis (Pitkänen *et al*., 1998), and amygdala volume is reduced by up to 43% in temporal lobe epilepsy (Pitkänen *et al*., 1998).

Of the various subnuclei of the amygdala, the lateral and basolateral nuclei displayed the most severe histochemical (Yilmazer-Hanke *et al*., 2000) and morphological alterations (Aliashkevich *et al*., 2003). The lateral nucleus gives rise to major projections to the hippocampal and parahippocampal regions (Pitkänen *et al*, 2000), which are also implicated in seizure generation and spread (Sloviter, 1996; Avoli *et al*., 2002).

Animal models of temporal lobe epilepsy have confirmed histopathological changes in the amygdaloid subnuclei overlapping with those in human temporal lobe epilepsy (Pitkänen *et al*., 1998), and have additionally demonstrated the vulnerability of somatostatin-containing γ-aminobutyric acid (GABA) containing neurons (Tuunanen *et al*., 1996). A decrease in inhibitory GABAergic synaptic influence has indeed been a critical element contributing to hyperexcitability of amygdala synaptic circuits in experimental models of epilepsy (Klueva *et al*., 2003; Benini and Avoli, 2006). Another line of evidence points to glutamatergic mechanisms underlying synaptic hyperexcitability in the amygdala in epilepsy (Shoji *et al*., 1998; Graebenitz *et al*., 2010). Overall, available evidence suggests an increase in excitation/inhibition ratio and state of hyperexcitability of synaptic circuits in the amygdala during seizure development and maintenance.

Surprisingly, little is known about alterations in density and/or subunit composition of neurotransmitter receptors in relation to the epileptic amygdala. Kainate and adenosine A_1 receptor densities are decreased in pentylenetetrazole-treated rats (Cremer *et al*., 2009). Levels of GluR2 α-amino-3-hydroxy-5-methyl-4-isoxazolepropionic acid (AMPA) receptor subunits were reduced 24 h, but not 1 week or 1 month after the last stage 5 seizure in amygdala-kindled rats (Prince *et al*., 1995). The messenger ribonucleic acids (mRNAs) for GluR1, GluR2 and GluR3 AMPA subunits were also decreased 24 h but not 1 month after the last hippocampal-kindled seizure (Lee *et al*., 1994). The α_1 $GABA_A$ receptor subunit is decreased in kindling-prone rats, but increased in slow-kindling rats (Gilby *et al*., 2005). Muscarinic cholinergic receptor densities are downregulated following systemic kainic acid administration (Schliebs *et al*., 1989). Finally, one study in epileptic patients found a reduction in serotonin 5-HT_{1A} receptor binding potential (Savic *et al*., 2004; Giovacchini *et al*., 2005).

Of note, conclusions on pathophysiological mechanisms in the amygdala related to temporal lobe epilepsy have been exclusively derived from experimental animal models. Only a single study is available that employed whole-cell patch-clamp techniques *in vitro* in surgical specimens of the amygdala obtained from patients with intractable temporal lobe epilepsy (Hüttmann *et al*., 2006). Intrinsic electrophysiological properties of putative projection neurons and local interneurons in the basolateral nucleus were reported in that study, but without a reference to synaptic interactions or pathophysiological mechanisms related to temporal lobe epilepsy. Therefore, we undertook a first study on synaptic network interactions and receptor profiles in the human amygdala, and their possible role in seizure generation.

Our study was performed on amygdaloid tissue that became available following surgical removal from patients with medically intractable temporal lobe epilepsy. Our experimental strategy was: (i) to assess basic patterns of activity *in vivo* through intra-operative recordings of field potentials from the exposed amygdala and hippocampus; (ii) to further characterize synaptic network interactions in the amygdala using field potential recordings in slices *in vitro* prepared from surgically resected specimens, with a focus on the lateral nucleus, which represents a major station of reciprocal connections with temporolimbic areas and a critical area for the spread of seizures in temporal lobe epilepsy (see above); and (iii) to determine the receptor fingerprints of major transmitter systems in the lateral nucleus through *in vitro* quantitative receptor autoradiography, and systematically compare data from surgical specimens of patients with temporal lobe epilepsy that had been physiologically characterized *in vitro* with those obtained from autopsy controls.

Materials and methods

Human amygdala tissue and intra-operative recordings

Patients suffering from intractable temporal lobe epilepsy were evaluated by extensive invasive and non-invasive methods to identify

the epileptic focus (Hufnagel *et al*., 2000; Kral *et al*., 2002). Neurosurgery was performed between 2005 and 2010. For all patients, the seizure focus was identified in the temporal lobe through conventional clinical procedures, consisting of epicortical electroencephalogram (EEG) recordings from the temporal superior gyrus, anamnesis and results from magnetic resonance imaging (MRI) scans. Removal of the amygdala was clinically indicated to achieve seizure control in all cases. Tissue containing the amygdala was obtained during therapeutical standard partial lobectomies from 26 patients with pharmacoresistant temporal lobe epilepsy (Hüttmann *et al*., 2006).

Detailed data of patients concerning seizure history, medication, MRI, histopathological findings and number of slices obtained from surgical specimens that were used for electrophysiological recordings and for receptor autoradiographic analysis are given in Table 1. Pathological examination revealed sclerosis of grade III in the hippocampus, whereas the amygdala was free of sclerosis, or in some cases, at sclerosis level I (Wyler *et al*., 1992). Of note, sclerosis was not detected in resected specimens *in vitro* used for electrophysiological and receptor autoradiographic studies. Patient data (gender, seizure type, MRI, histopathological findings, slice activity) and absence/presence of sclerosis were encoded as 0 and 1, respectively, and correlation analysis was performed using the non-parametric Spearman's rho test.

In addition to the epicortical EEG, depth recordings of the EEG were obtained intra-operatively from the exposed surface of the amygdala and hippocampus, respectively, by using conventional stripe electrodes (Type ES-4 P-7, Ad-TECH) in three patients. All procedures were approved by the local ethics committee (Approval No. 2008-151-f-S, Ethikkommission der Ärtzekammer Westfalen-Lippe und der Medizinischen Fakultät der Westfälischen Wilhelms-Universität Münster) and informed consent was obtained from all patients.

Control amygdala tissue for receptor autoradiographic studies was obtained at autopsy from the body donor programme of the Centre of Anatomy and Brain Research, University of Düsseldorf. Subjects ($n = 5$; two males) had no known history of neurological or psychiatric diseases. Mean age was 74 ± 4 years and causes of death were cardiac arrest ($n = 3$), cardiorespiratory insufficiency ($n = 1$) and multiple organ failure ($n = 1$).

Slice preparation

The blocks of resected tissue consisted of the amygdala and surrounding tissue (10–15 mm^3). Slices were prepared from a block of the amygdala within 5 min of tissue resection. The general techniques for slice preparation (Hüttmann *et al*., 2006) and transport (Köhling *et al*., 1996) have been described in detail elsewhere. Briefly, amygdala slices of 400–500 μm thickness were cut using a vibratome (MA-752 Motorized Advance Vibroslice, Campden Instruments Ltd) in the operation theatre. From an individual specimen, alternate sections were used for identification of amygdaloid nuclei and assessment of overall tissue preservation, for receptor autoradiography and for electrophysiological recordings. Slices used for histological and receptor autoradiographic analysis were frozen at −40°C in isopentane and stored at −80°C until further processing. Those used for electrophysiological recordings were immediately placed in a portable incubation chamber (Köhling *et al*., 1996) with oxygenated (95% O_2, 5% CO_2) artificial cerebrospinal fluid (CSF) at 28°C and pH 7.4. During and after transport from the surgery theatre to the electrophysiological facilities, slices were allowed to recover for a period of 1–2 h before transfer into a submerged recording chamber. The composition of the artificial CSF was (in mM): NaCl 124; KCl 4; $CaCl_2$ 2; NaH_2PO_4 1.24; $MgSO_4$ 1.3; $NaHCO_3$ 26; and glucose 10. In the recording chamber, the temperature was raised to 33°C. During the experiments, pH, temperature and flow rate (4 ml/min; bath volume 1 ml) were continuously monitored. Following termination of electrophysiological experiments, slices were frozen at −40°C in isopentane, and stored at −80°C until further processing for histological verification of recording sites and autoradiographic analyses for receptor fingerprints (see below). Slices from all patients, except for Patient 7 whose data had to be discarded because of reconstruction work in the Münster lab, were screened for spontaneous versus non-spontaneous activity. Of those, slices from a total of 11 patients were electrophysiologically tested in detail (multiple site recordings, pharmacological experiments; see below). Of these 11 patients, all were prepared for histology and nine for receptor autoradiography (two were excluded for technical reasons).

Electrophysiological recordings

Extracellular field potential recordings were performed in the lateral nucleus using glass microelectrodes (Borosilicate glass capillaries with filament, Code No. 1403512, Hilgenberg), pulled to resistances of 0.5–1.5 MΩ when filled with artificial CSF. To search for spontaneous activity, recordings were simultaneously obtained from two sites in a given slice, and the two recording electrodes were periodically repositioned following an imaginary position grid consisting of squares ~500 μm across. Recordings lasted between 3.8 and 19.7 min (on average 10.1 min) at sites showing spontaneous activity, and a minimum period of 10 min was allowed to detect spontaneous activity at any given site. Recorded waveforms were fed through a custom-made amplifier (Koch *et al*., 2005), low-pass filtered at 10 kHz and stored on a personal computer via an AD/DA interface (Digidata 1322A, Molecular Devices). Recordings were visualized online by using the software AxoScope 6 (Molecular Devices).

Pharmacologically active substances were dissolved in artificial CSF and added to the superfusate. Drugs applied were: the *N*-methyl-D-aspartate (NMDA) and AMPA receptor antagonists DL-2-amino-5-phosphono-valerate (APV, 50 μM; Sigma-Aldrich) and 6-cyano-7-nitro-quinoxaline-2,3-dione (CNQX, 10 μM; RBI), respectively, and the $GABA_A$ receptor antagonist bicuculline methiodide (10 μM; Sigma-Aldrich).

Data analysis and electrophysiological data statistics

Field potential recordings were analysed off-line using Spike2 5.15 software (Cambridge Electronic Design Ltd). Interictal-like events were detected after filtering recorded waveforms, using a 50 Hz digital low-pass filter, by means of an amplitude threshold adjusted to three times the amplitude of the noise for each recorded channel. Amplitudes of detected events were then measured peak-to-peak on the unfiltered recorded waveforms. Average frequency and amplitude of spontaneously occurring events were determined under a given experimental condition (before, during application and following washout of a drug), and for each recording site in an individual slice. Activity was analysed over a minimal period of 8 min for each experimental condition. The effect of an applied drug was considered maximal once a stable effect was obtained. Recordings were obtained from sites displaying stable interictal-like activity under drug-free conditions. Activity was compared during application and following

Table 1 Patient data

Case	Gender	Age (years)	Febrile conv.	Seizure type	Seizures/ month	Seizure for *n* years	MRI and histopathology	Anti-epileptic drugs	Slice activity	Total slices for E-phys/sp slices (*n*)	Total slices taken for RA /sp slices (*n*)
1	Female	49	–	PS, GS	12	39	Sclerosis, gliosis, dysplasia, AHS	CBZ, LEV, VPA	sp		
2	Male	34	–	PS, GS	3	28	Sclerosis, AHS	CBZ, DPH, GPT, LEV, LTG, MSX, OCBZ, PHB, VGB, VPA	sp, nsp		
3	Female	55	–	PS, GS	12	35	Sclerosis, gliosis, astrocytosis, AHS	CBZ, LEV, LTG	nsp		
4[a]	Female	13	–	PS	60	7	Mesial atrophy, sclerosis, gliosis, dysplasia	CBZ, OCBZ, VPA	sp, nsp	4/1	
5	Female	44	+	PS, GS	300	22	Sclerosis, gliosis, atrophy, AHS	GPT, LEV, OCBZ, VPA	nsp		
6[b]	Female	47	–	PS	2	30	Sclerosis, gliosis, astrocytosis, AHS	DPH, LEV, LTG	nsp		
7[b]	Male	18	–	PS	2	3	Atrophy, dysplasia, lesion, sclerosis, astrocytosis, AHS	CBZ, OCBZ, VPA	Not tested		
8[a]	Female	14	–	PS	20	12	Lesion, sclerosis, AHS	CBZ, ETX, LEV, LTG, OCBZ, STM	sp	1/1	
9[b]	Female	36	–	PS	4	30	Lesion, sclerosis, gliosis, astrocytosis, dysplasia, lam disorder, AHS	CBZ, LEV, LTG, OCBZ, TGB, VPA	sp		
10	Male	50	+	PS, GS	1	26	Dysplasia, AHS	ACTH, BROM, CBZ, CZ, DPH, ETX, GPT, LTG, MSX, OCBZ, PHB, PRM, STM, TGB, VGB, VPA	nsp		
11	Male	46	–	PS, GS	8	39	Mesial atrophy, astrocytosis, dysplasia, AHS	CBZ, ETX, LEV, LTG, PHB, PHT, STM, VPA	nsp		
12	Male	42	+	PS, GS	40	6	Mesial atrophy, tumour, astrocytosis, dysplasia, atrophy, AHS	CBZ, LEV, PHT	nsp		
13	Female	55	+	PS, GS	7	43	AHS	CBZ, DPH, LEV, PRM, VPA	sp, nsp		
14	Female	15	–	PS, GS	120	3	Sclerosis, dysplasia	LEV, LTG, OCBZ, STM, VPA	nsp		
15	Male	7	–	PS, GS	45	6	Lateral atrophy, dysplasia	CBZ, LEV, LTG, STM, VPA	nsp		
16	Female	58	–	PS	16	35	Sclerosis, AHS	CBZ, LEV, VPA	nsp		
17[a,c]	Female	65	+	PS, GS	7	38	Sclerosis, AHS	CBZ, GPT, PHB, PHT, VGB	nsp	4/0	1/0
18[a,c]	Male	45	–	PS, GS	2	4	Ø	CBZ, LEV	sp, nsp	3/2	1/1
19[a,c]	Female	29	–	PS, GS	5	15	Ø	LEV, LTG, OCBZ, VPA	sp, nsp	$4/3,1^{sp}_{after\ bic}$	2/1
20[a,c]	Female	40	–	PS, GS	12	39	Sclerosis	CBZ, LEV, OCBZ, PRM, VPA	nsp	3/0	1/0
21[a,c]	Male	21	–	PS, GS	2	n.g.	Sclerosis	CBZ, LEV, LTG, VPA	nsp	1/0	1/0
22[a,c]	Female	54	–	PS	2	8	Lesion, sclerosis	CBZ, LTG, OCBZ	nsp	2/0	1/0
23[a,c]	Female	40	–	PS, GS	8	12	Sclerosis	CBZ, DPH, LEV, LTG, OCBZ	sp, nsp	3/2	3/2
24[a,c]	Female	44	–	PS, GS	3	15	Mesiale atrophy	CBZ, GPT, LEV, VPA, PGB	sp, nsp	4/1	3/1
25	Male	54	–	PS, GS	2	18	Sclerosis	LEV, LTG, OCBZ, PHT, VPA	nsp		
26[a,c]	Male	18	+	PS, GS	7	8	Sclerosis, dysplasia	LEV, LTG, PHT	nsp	1/0	1/0

The column 'Slice activity' indicates the results of the first global screening for activity for each case. If all slices tested in a given case were spontaneously active, the case was called spontaneous (sp). If all slices tested were not spontaneously active, the case was called non-spontaneous (nsp). If a case showed both types of slices activity, i.e. spontaneously and not spontaneously active, the case was called sp, nsp. The column 'Total number of slices for electrophysiology/spontaneously active slices' indicates, for each case from which a slice is taken into this study, how many slices in total were screened for activity and how many of those were spontaneously active. The column 'Total number of slices taken for receptor autoradiography/spontaneously active slices' indicates, for cases taken for receptor autoradiographic analysis and from which field potentials recordings are included in this study, the total number of slices used for receptor autoradiographic analysis and how many of those were spontaneously active.

[a]Cases with slices used for field potential recordings.

[b]Cases used for intra operative recordings.

[c]Cases with slices used for receptor autoradiography.

ACTH = adrenocorticotropic hormone; AHS = Ammon's horn sclerosis; bic = bicuculline; BROM = bromide; CBZ = carbamazepine; conv. = convulsions; CZ = clobazam; DPH = diphenyhydantoin; E-phys = electrophysiology; ETX = ethosuximide; GPT = gabapentin; GS = generalized seizures; LEV = levetiracetam; LTG = lamotrigin; m = male; MSX = mesuximide; n.g. = not given; Ø = no information; OCBZ = oxcarbazepine; PHB = phenobarbital; PHT = phenytoin; PRM = primidone; PS = partial seizures; RA = receptor autoradiography; sp, nsp = appearance and non-appearance of spontaneous epileptiform field potentials (spikes and/or sharp waves) in corresponding slice preparation; STM = sultiam; TGB = tiagabine; VGB = vigabatrin; VPA = valproate

washout of the $GABA_A$ receptor antagonist bicuculline (10 μM), the NMDA receptor antagonist APV (50 μM) and the AMPA receptor antagonist CNQX (10 μM). Amplitude and frequencies of field potentials obtained under each pharmacological condition were compared between groups. In addition under drug-free control conditions, inter-event intervals and instantaneous frequencies were determined from single events. Cross-correlation analysis was performed for each pair of simultaneously recorded events (time window width of 600 ms, offset ±300 ms, bin size 10 ms, trigger CH2). The percentage of correlated events was then calculated from the number of events within ±100 ms around zero divided by the total number of events within the 600 ms window, multiplied by 100. Power spectra of recorded waveforms were constructed for frequencies below 50Hz by using Fast Fourier Transform with increments of 0.1Hz. Data are given as mean ± SEM.

Statistical analysis was done using Prism5 (GraphPad software) and PASW 18 (IBM Corporation 2010). Parameters characterizing spontaneous epileptiform field potentials were first tested for normal distribution by using the Kolmogorov–Smirnov normality test. Further, statistical significance was assessed with one-way ANOVA followed by Tukey's multiple comparison test, or Kruskall–Wallis followed by Dunn's multiple comparison test, as applicable. Fast Fourier Transform data were tested for statistical differences using two-way ANOVA followed by Bonferroni *post hoc* tests. Differences are considered significant at $\leqslant 0.05$.

Identification of recording sites

Data were only included in the analysis if recording sites had been verified in the lateral nucleus of the laterobasal group of the amygdala, as defined by Heimer *et al*. (1999).

For histological verification of recording sites, individual slices were deep frozen in isopentane, flat mounted, serially resectioned at −20° C in 10 μm thick sections using a cryostat (Leica) and thaw mounted. Every 11th section was used for the visualization of cell bodies, every 12th for the visualization of myelin sheaths and the remaining ones were processed for receptor autoradiography (see below). For each recorded slice, histologically processed sections were superimposed onto photographs of the slice during electrophysiological recording and landmarks such as fibre tracts and marks left by stimulation electrodes were carefully matched.

Sections were stained for cell bodies with a modified silver method (Merker, 1983). Sections were air-dried, fixed overnight in Bodian fixative, treated with 4% formic acid and incubated overnight in 10% formic acid/30% peroxide. Sections were then thoroughly washed and immersed in 1% acetic acid (2 × 5 min). They were then placed in a physical developer under constant movement for ∼10 min until cell bodies were dark grey/black. Development was terminated by a wash in 1% acetic acid (2 × 5 min) and subsequently fixed 5 min in a T-Max fixative (Kodak Europe).

Myelin sheaths were silver stained according to the protocol described by Gallyas (1979). Briefly, sections were air-dried and fixed overnight in a buffered formalin solution. Sections were then thoroughly washed and immersed for 30 min in a 2/1 mixture of pyridine and acetic anhydride. After being washed (2 × 5 min), sections were incubated in the dark in an ammonium silver nitrate solution for 1 h, and immersed in 1% acetic acid (3 × 3 min). Sections were then placed in a physical developer under constant movement for ∼10 min until myelin sheaths were dark brown/black. Development was terminated by a 5 min wash under running water.

For both staining methods, sections were dehydrated in ascending grades of alcohol (70, 96 and 100%) followed by two immersions in xylene (5 min for each step) before coverslipping with DePex.

Receptor autoradiography

Sections destined to quantitative *in vitro* receptor autoradiography were processed for the visualization of glutamatergic (AMPA, kainate, NMDA, mGluR2/3), GABAergic ($GABA_A$, $GABA_B$), serotonergic ($5HT_{1A}$, $5HT_2$), cholinergic (muscarinergic M_1, M_2, M_3, nicotinic), noradrenergic (α_1, α_2), dopaminergic (D_1) and adenosinergic (A_1) receptors by incubation in solutions containing the respective tritiated ligands according to standard procedures (Table 2) (Zilles *et al*., 1999; Palomero-Gallagher *et al*., 2009). For a given tritiated ligand, all sections of all probes (epileptic cases and control tissue) were processed in a single incubation session. The incubation comprises a pre-incubation step to remove the endogenous ligand from the section, a main incubation step to label the receptor binding sites with a tritiated ligand in the presence (non-specific binding) or absence (total binding) of an appropriate non-labelled displacer, and a final rinsing step to eliminate unbound radioactive molecules and buffer. A non-specific binding of <5% of the total binding was found under these conditions. Therefore, the total binding was considered an acceptable estimate of the specific binding.

The tritium-labelled sections were co-exposed for 10–15 weeks against [^{3}H]-sensitive film (Kodak BioMax MR film) together with plastic [^{3}H]-standards (Microscales) of known, step-wise increasing concentrations of radioactivity. Grey values in developed films were measured with an image analysis system as previously reported (Zilles *et al*., 2002*b*). A comparison of the grey values caused by the tritium-labelled tissue sections with those of the tritium-labelled plastic standards allows the transformation of grey values to concentrations of radioactivity, and finally, to mean binding site densities per protein unit (fmol/mg protein). Briefly, actual concentrations of radioactivity were multiplied by $(K_D + c)/c$ to obtain B_{max} values (B_{max}, binding site concentrations at saturation of the ligand–receptor complexes; K_D, equilibrium dissociation constant of ligand-binding kinetics; c, actual incubation concentration of labelled ligand). For further details, see Zilles *et al*. (2002*a*).

Average binding site densities ±SEM were calculated for each ligand and section. The complex co-distribution patterns of various receptors in the lateral nucleus was comprehensively visualized by so-called 'receptor fingerprints', i.e. polar coordinate plots of the mean regional densities of different receptors binding sites in a single, cytoarchitectonically defined brain region (Zilles *et al*. 2002*a*, *b*).

Statistical analysis of autoradiography data

Since the number of binding sites ($n = 20$) exceeded the number of slices investigated ($n = 14$), the data on binding sites density originating from the receptor autoradiography were subjected to a principal component analysis, and only those components with eigenvalues $\geqslant 1$ were used for testing the hypothesis of a grouping of the data, i.e. to test whether the three types of tissue (control, spontaneously and non-spontaneously active epileptic cases) were homogenous or if at least one pair differed significantly. We performed a discriminant analysis to determine whether experimental groups differed as a whole from each other. In the case of a positive answer, we performed *post hoc* univariate *F*-tests to determine which of the examined ligands

Table 2 Ligands used for receptor autoradiography

Transmitter system	Receptor	Ligand (c in nM)	Pharmacology	K_D (nM)	Displacer	Incubation buffer	Pre-incubation (minutes, °C)	Main Incubation (minutes, °C)	Final rinsing
Glutamatergic	AMPA	[^{3}H]-AMPA (10.0)	Agonist	10.0	Quisqualate (10 μM)	50 mM Tris–acetate (pH 7.2) [+100 mM KSCN][a]	3 × 10, 4	45, 4	(i)[b] 4 × 4 s, 4°C (ii) acetone glutaraldehyde (100 ml + 2.5 ml), 2 × 2 s, 22°C
	kainate	[^{3}H]-Kainate (9.4)	Agonist	12.0	SYM 2081 (100 μM)	50 mM Tris–acetate (pH 7.1) [+10 mM Ca^{2+}-acetate][a]	3 × 10, 4	45, 4	(i)[b] 3 × 4 s, 4°C (ii) acetone glutaraldehyde (100 ml + 2.5 ml), 2 × 2 s, 22°C
	NMDA	[^{3}H]-MK-801 (3.3)	Antagonist	5.0	(+)MK-801 (100 μM)	50 mM Tris–acetate (pH 7.2) + 50 μM glutamate [+30 μM glycine + 50 μM spermidine][a]	15, 4	60, 22	(i)[b] 2 × 5 min, 4°C (ii) 1 dip in distilled water, 22°C
	mGluR2/3	[^{3}H]-LY 341 495 (1.0)	Antagonist	4.0	L-Glutamate (1 mM)	10 mM phosphate buffer (pH 7.6) [+100 mM KBr][a]	2 × 5, 22	60, 4	(i)[b] 2 × 5 min (ii) 1 dip in distilled water, 22°C
GABAergic	$GABA_A$	[^{3}H]-Muscimol (7.7)	Agonist	6.0	GABA (10 μM)	50 mM Tris–citrate (pH 7.0)	3 × 5, 4	40, 4	(i)[b] 3 × 3 s, 4°C (ii) 1 dip in distilled water, 22°C
	$GABA_A$	[^{3}H]-SR95531 (3.0)	Antagonist	6.0	GABA (1 mM)	50 mM Tris–citrate (pH 7.0)	3 × 5, 4	40, 4	(i)[b] 3 × 3 s, 4°C (ii) 1 dip in distilled water, 22°C
	$GABA_B$	[^{3}H]-CGP 54626 (2.0)	Antagonist	1.48	CGP 55845 (100 μM)	50 mM Tris–HCl (pH 7.2) + 2.5 mM $CaCl_2$	3 × 5, 4	60, 4	(i)[b] 3 × 2 s, 4°C (ii) 1 dip in distilled water, 22°C
	BZ	[^{3}H]-Flumazenil (1.0)	Antagonist	2.0	Clonazepam (2 μM)	170 mM Tris–HCl (pH 7.4)	15, 4	60, 4	(i)[b] 2 × 1 min, 4°C (ii) 1 dip in distilled water, 22°C
Serotoninergic	$5\text{-}HT_{1A}$	[^{3}H]-8-OH-DPAT (1.0)	Agonist	2.0	5-Hydroxy-tryptamine, (1 μM)	170 mM Tris–HCl (pH 7.4) [+4 mM $CaCl_2$ + 0.01% ascorbate][a]	30, 22	60, 22	(i)[b] 5 min, 4°C (ii) 3 dips in distilled water, 22°C
	$5\text{-}HT_2$	[^{3}H]-Ketanserin (1.14)	Antagonist	0.5	Mianserin (10 μM)	170 mM Tris–HCl (pH 7.7)	30, 22	120, 22	(i)[b] 2 × 10 min, 4°C (ii) 3 dips in distilled water, 22°C
Cholinergic	M_1	[^{3}H]-Pirenzepine (1.0)	Antagonist	3.0	Pirenzepine (2 μM)	Modified Krebs buffer (pH 7.4)	15, 4	60, 4	(i)[b] 2 × 1 min, 4°C (ii) 1 dip in distilled water, 22°C
	M_2	[^{3}H]-Oxotremorine-M (1.7)	Agonist	0.8	Carbachol (10 μM)	20 mM HEPES–Tris (pH 7.5) + 10 mM $MgCl_2$ + 300 nM Pirenzepine	20, 22	60, 22	(i)[b] 2 × 2 min, 4°C (ii) 1 dip in distilled water, 22°C

(continued)

Table 2. Continued

Transmitter system	Receptor	Ligand (c in nM)	Pharmacology	K_D (nM)	Displacer	Incubation buffer	Pre-incubation (minutes, °C)	Main Incubation (minutes, °C)	Final rinsing
	M_2	[^{3}H]-AF-DX384 (5.0)	Antagonist	2.0	Atropine sulphate (100 μM)	Krebs buffer (pH 7.4) 4.7 mM KCl + 120 mM NaCl + 1.2 mM $MgSO_4$ + 1.2 mM KH_2PO_4 + 5.6 mM D-Glucose + 25 mM $NaHCO_3$ + 2.5 mM $CaCl_2$	15, 22	60, 22	(i)[b] 3 × 4 min, 4°C (ii) 1 dip in distilled water, 22°C
	M_3	[^{3}H]-4-DAMP (1.0)	Antagonist	0.2	Atropine sulphate (10 μM)	50 mM Tris–HCl (pH 7.4) + 0.1 mM PSMF + 1 mM EDTA	15, 22	45, 22	(i)[b] 2 × 5 min, 4°C (ii) 1 dip in distilled water, 22°C
	AChN	[^{3}H]-Epibatidine (0.5)	Agonist	0.07	Nicotine (100 μM)	15 mM HEPES (pH 7.5) + 120 mM NaCl + 5.4 mM KCl + 0.8 mM $MgCl_2$ + 1.8 mM $CaCl_2$	20, 22	90, 22	(i)[b] 5 min, 4°C (ii) 1 dip in distilled water, 22°C
Noradrenergic	α_1	[^{3}H]-Prazosin (0.2)	Antagonist	0.2	Phentolamine Mesylate (10 μM)	50 mM Na/K-phosphate buffer (pH 7.4)	15, 22	60, 22	(i)[b] 2 × 5 min, 4°C (ii) 1 dip in distilled water, 22°C
	α_{2h}	[^{3}H]-UK 14,304 (0.64)	Agonist	1.4	Phentolamine Mesylate (10 μM)	50 mM Tris–HCl + 100 μM $MnCl_2$ (pH 7.7)	15, 22	90, 22	(i)[b] 5 min, 4°C (ii) 1 dip in distilled water, 22°C
	α_2	[^{3}H]-RX 821002 (1.4)	Antagonist	2.8	Phentolamine Mesylate (10 μM)	50 mM Tris–HCl + 100 μM $MnCl_2$ (pH 7.7)	15, 22	90, 22	(i)[b] 5 min, 4°C (ii) 1 dip in distilled water, 22°C
Dopaminergic	D_1	[^{3}H]-SCH 23390 (1.67)	Antagonist	0.14	SKF 83566 (1 μM)	50 mM Tris–HCl + 120 mM NaCl + 5 mM KCl + 2 mM $CaCl_2$ + 1 mM $MgCl_2$ (pH 7.4)	20, 22	90, 22	(i)[b] 2 × 20 min, 4°C (ii) 1 dip in distilled water, 22°C
Adenosine	A_1	[^{3}H]-DPCPX (1.0)	Antagonist	0.5	R-PIA (100 μM)	170 mM Tris–HCl + 2 U/l Adenosine deaminase [+ Gpp(NH)p (100 μM)][b] (pH 7.4)	15, 4	120, 22	(i)[b] 2 × 5 min, 4°C (ii) 1 dip in distilled water, 22°C

a Only for main incubation buffer.
b Washed in the incubation buffer.

contributed to this significance. For all tests, statistical significance was set at $P < 0.05$.

Results

Intra-operative recordings

Intra-operative recordings were performed in three patients during surgical treatment of refractory temporal lobe epilepsy (Fig. 1A). The EEG from the amygdala and hippocampus were recorded together with the EEG from the superior temporal gyrus. In two patients, interictal activity appeared as synchronous spikes, spike-and-waves and polyspike wave complexes in EEG recordings from the amygdala and the hippocampus, but not from the cortex (Fig. 1B). The frequency of interictal activity, as averaged over a period of 10 min, was 0.023 and 0.09 Hz in the two patients, respectively. Frequency band analysis of EEGs from the amygdala indicated the presence of θ- and α-waves during most of the recording time, β waves were observed in one patient during 11% of the recording time (Fig 1C).

Properties of interictal-like activity in the lateral nucleus, *in vitro*

From a total of 26 patients, specimens from 11 patients allowed detailed electrophysiological analyses and histological verification of recording sites in individual sections. Figure 2 illustrates an example of histological verification of recording sites in individual slices. In a total of 30 slices, recording sites were histologically verified in the lateral nucleus, and only those were included in

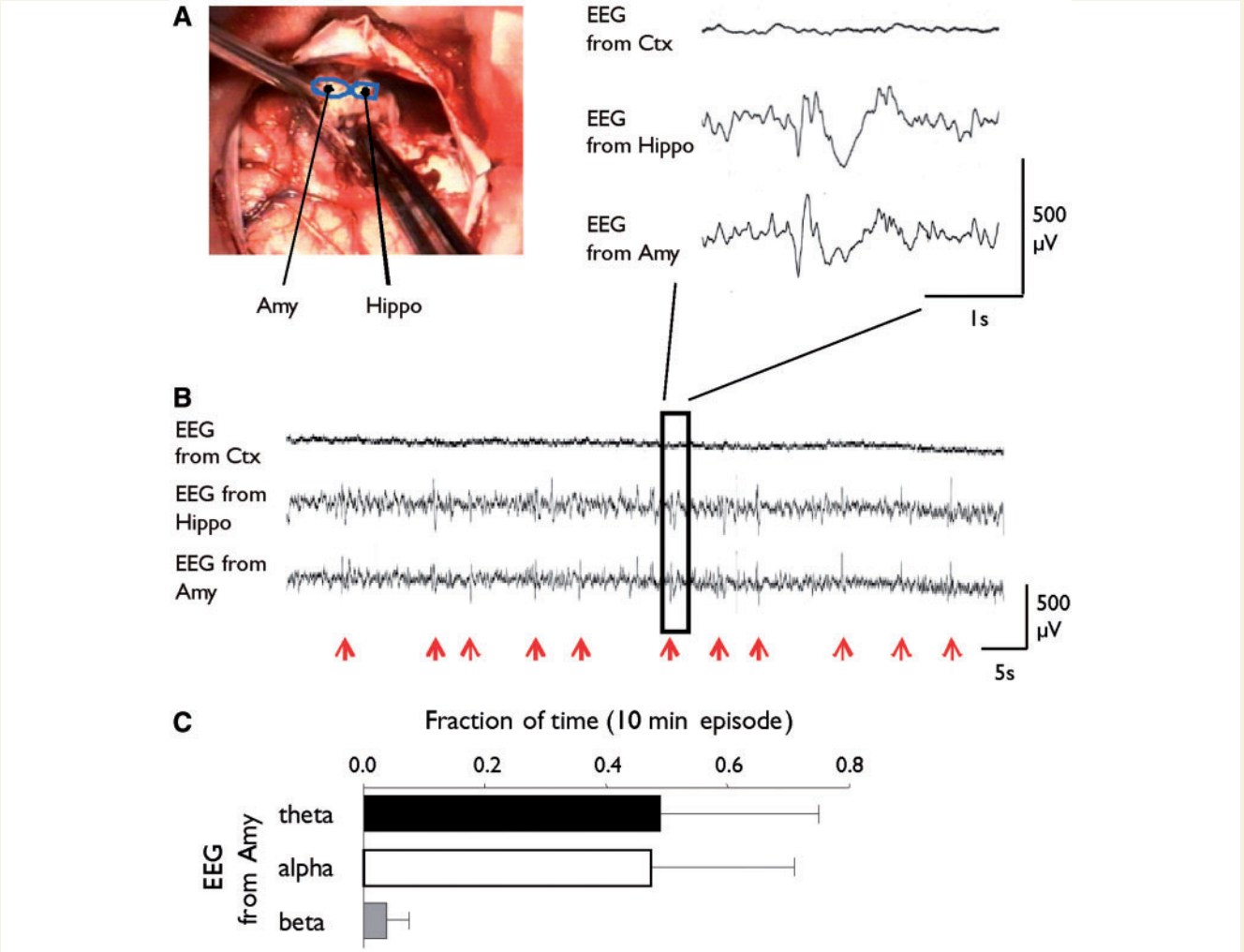

Figure 1 Intra-operative recordings *in vivo*. (**A**) Exposed surface of the amygdala and hippocampus for recordings of EEG from the amygdala and hippocampus with stripe electrodes (*left*). (**B**) Example traces of simultaneous EEG from the cortex, the amygdala and from the hippocampus from recording in (**A**). Red arrows indicate spike-wave discharges. Period depicted at an enlarged time scale as indicated. Note occurrence of a spike-wave discharge in the EEG from the hippocampus and amygdala, but not in that from the cortex. (**C**) Frequency analysis of the EEG from the amygdala during a 10 min recording episode (from three patients). Amy = amygdala; Ctx = cortex; Hippo = hippocampus.

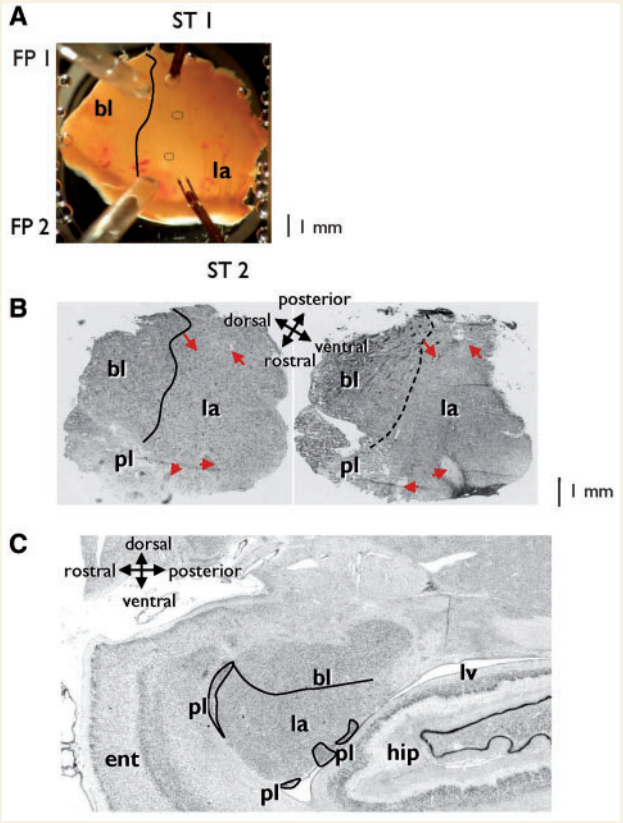

Figure 2 Anatomical reconstruction of the amygdala. (**A**) Photograph of an individual slice prepared from a surgical specimen of the amygdala, after positioning in the recording chamber. Two stimulation electrodes (ST1 and ST2) and two field potential recording electrodes (FP1 and FP2, circles represent the approximate position of the tip in the slice) positioned in the putative lateral nucleus. (**B**) Photographs of the same individual slice, after resectioning for cell body staining (*left*) and myelin staining (*right*) to verify location of stimulation and recordings sites (marked by red arrows). Solid and dashed lines indicate the border between the lateral and basolateral nuclei. (**C**) Anatomical reconstruction of a larger slice containing the amygdala and neighbouring hippocampal and entorhinal cortical regions. Bl = basolateral nucleus of the amygdala; ent = entorhinal cortex; hip = hippocampus; la = lateral nucleus of the amygdala; lv = lateral ventricle; pl = nucleus paralaminaris of the amygdala.

the analyses. Simultaneous recordings at two sites within the lateral nucleus and periodic repositioning of the recording electrodes following an imaginary position grid consisting of squares ~500 μm across revealed the existence of spontaneous electrical activity in the lateral nucleus of six patients (detected in 11 slices). Recording period at a given site averaged to 10.1 min (range 3.8–19.7 min). An example of spontaneous electrical activity is illustrated in Fig. 3, and an overview of the slice activity is provided in Table 1 for each patient. In field potential recordings, spontaneous activity appeared as monophasic or biphasic events, often with superimposed population spikes (Fig. 3A and B). Activity was localized, in that it occurred at one to several sites in different lateral nucleus slices, with various degrees of synchronization (Fig. 3B). Polarity of the field potentials was constant at a given recording site, but varied between recording sites (Fig. 3A and B).

Representative activity (total of 4598 spontaneous events) from a sample of 20 recording sites (seven slices, six patients) was analysed in detail. Amplitudes of spontaneous events ranged from 14 to 290 μV (average 71.4 ± 0.9 μV), and inter-event intervals ranged from 0.19 to 307 s (2.01 ± 0.10 s), corresponding to instantaneous frequencies ranging from 0.01 to 5.31Hz (0.84 ± 0.006Hz). Of all analysed events, 75% had inter-event intervals below 1.72 s (instantaneous frequencies below 1.01Hz). Cross-correlation analysis revealed a correlation of 66.7 ± 14.9% between simultaneously recorded events. Fourier transform analysis demonstrated a significant difference in power spectra between recordings obtained from spontaneously and non-spontaneously active slices (samples of seven slices with and six slices without spontaneous activity from six patients each) in the low frequency domain, ranging from 0.1 to 1.5 Hz (two-way ANOVA: interaction: not significant (ns); group: $P < 0.0001$; frequency: $P < 0.0001$; Bonferroni *post hoc* test for 0.1 to 1.5Hz: $P < 0.05$). In some slices, potentials were evoked with extracellular electrical micro-stimulation and gained in amplitude with increasing stimulation strength until reaching a maximum (data not shown). Both the polarity and shape of evoked potentials were similar to those of spontaneous potentials.

Importantly, the occurrence of spontaneous activity was not correlated with gender, age, seizure history or anti-epileptic medication of the patients. However, it was negatively correlated with the presence of sclerosis as detected by MRI ($r_{\text{Spearman's rho}} = -0.559$; $P = 0.04$).

Pharmacological properties of interictal-like activity

In order to elucidate the nature of the receptors participating in the generation of the interictal-like activity, glutamatergic and $GABA_A$ receptor blockers were tested. Recordings were obtained from a total of eight recording sites displaying stable interictal-like activity under drug-free conditions (four slices from three patients), and activity was compared before, during application and following washout of the $GABA_A$ receptor antagonist bicuculline (10 μM). Upon return of interictal-like activity to control levels, the NMDA receptor antagonist APV (50 μM) and the AMPA receptor antagonist CNQX (10 μM) were tested (four recordings sites, two slices from two patients). Overall, the drugs had a significant effect on average amplitude and frequency of interictal-like events, when compared with drug-free conditions, as shown by one-way ANOVA [$GABA_A$ receptor blockade: amplitude, $F(3,34) = 24.42$, $P < 0.0001$; frequency, $F(3,31) = 4.54$, $P = 0.01$] and by the Kruskal–Wallis test (glutamate receptor blockade: amplitude, $K = 10.06$, $P = 0.018$; frequency, $K = 10.81$, $P = 0.013$).

Application of the $GABA_A$ receptor antagonist bicuculline (10 μM) readily abolished interictal-like activity at all sites tested (Fig. 4A). During washout of the drug, spontaneous field potentials reappeared with significantly increased amplitude of the events (Control versus bicuculline wash early, $P < 0.001$; 5418

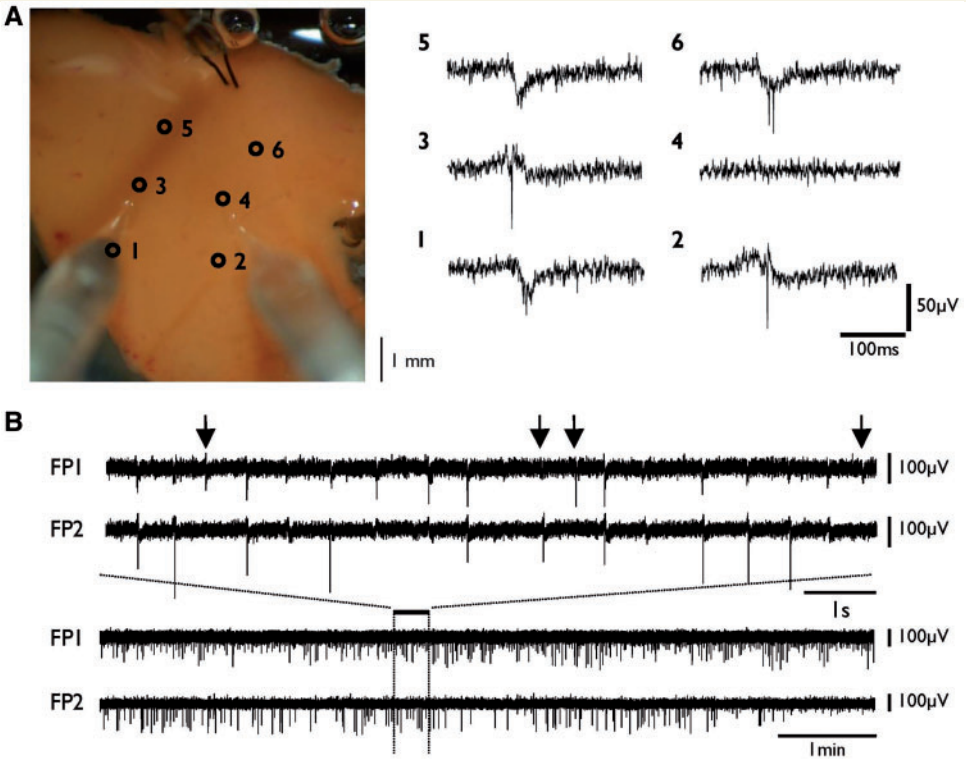

Figure 3 Field potential recordings, *in vitro*. (**A**) Slice preparation of the lateral amygdala, indicating sites of local field potential recordings, obtained simultaneously from two sites in three recording sessions (sites marked with 1–2, 3–4 and 5–6). Examples of local field potentials at sites indicated are illustrated on the *right*. (**B**) Local field potentials recorded simultaneously at two sites (1, 2) over longer periods, depicted at two different time scales. Note the occurrence of spontaneous interictal-like activity synchronously or non-synchronously (examples marked by arrows) at the two recording sites.

analysed events) but unchanged frequency as compared with control conditions during early stages of washout (Fig. 4A). At later stages (>17 min), amplitudes and frequencies of interictal-like events went back to control levels before drug application (Fig. 4). Subsequent application of the NMDA receptor antagonist APV (50 μM) had no significant effect, whereas addition of the AMPA receptor antagonist CNQX (10 μM) reversibly blocked interictal-like activity (Fig. 4B).

In addition, the power spectra of interictal-like activity was affected by the tested receptor antagonists (two-way ANOVA: interaction: ns; drug: $P < 0.0001$; frequency: $P < 0.0001$). Both, bicuculline and CNQX abolished the peak at low frequencies (0.1–1.5Hz) in power spectra, which was found to distinguish recordings obtained from spontaneously versus non-spontaneously active sites in the lateral nucleus.

Receptor autoradiography

Receptor autoradiographic analysis was carried out in 9 out of the 11 cases used for electrophysiological recordings which had been anatomically proven to be in the lateral nucleus (Table 1). Out of these, four cases ($n = 5$ slices, Table 1) had been shown to be spontaneously active based on field potential analysis. Receptor autoradiographs demonstrating 20 binding sites of 17 different receptors belonging to seven neurotransmitters systems were evaluated, and the binding site densities were measured in the cytoarchitectonically defined lateral nucleus of the amygdala. In a first step, a correlation matrix of receptor densities was computed in order to merge variables by means of a factor analysis, and thus reduce our data set to the smallest possible number of uncorrelated characteristic describing factors. The factor analysis showed that the first five components accounted for 83% of the data variation. Only those ligands with a loading factor 1 larger than 0.5 were taken into account for the discriminant analyses. These ligands were: kainate (factor 1 = −0.9109), AMPA (factor 1 = −0.8573), SR95531 (factor 1 = 0.8002), 4-DAMP (factor 1 = 0.7933), oxotremorine-M (factor 1 = −0.6959), AF-DX384 (factor 1 = −0.6697), 8-cyclopentyl-1,3-dipropylxanthine (DPCPX) (factor 1 = 0.6211), LY 341 495 (factor 1 = −0.5756), prazosin (factor 1 = −0.5655) and ketanserin (factor 1 = 0.5648).

Epileptic cases showing spontaneous epileptiform potentials did not differ significantly from those without spontaneous discharges in their mean receptor densities (discriminant analysis; $P > 0.1$; Figs 5 and 8). Thus, no *post hoc* tests were carried out. In a next step, spontaneously and non-spontaneously active slices were pooled into a single group called 'epileptic'. Comparison of data from the epileptic group to that from autopsy controls using discriminant function analysis showed a highly significant separation of the two groups [$F(5, 13) = 68.15$; $P = 0.0000$; Figs. 6–8). *Post hoc* univariate *F*-tests revealed significant differences for 8 of

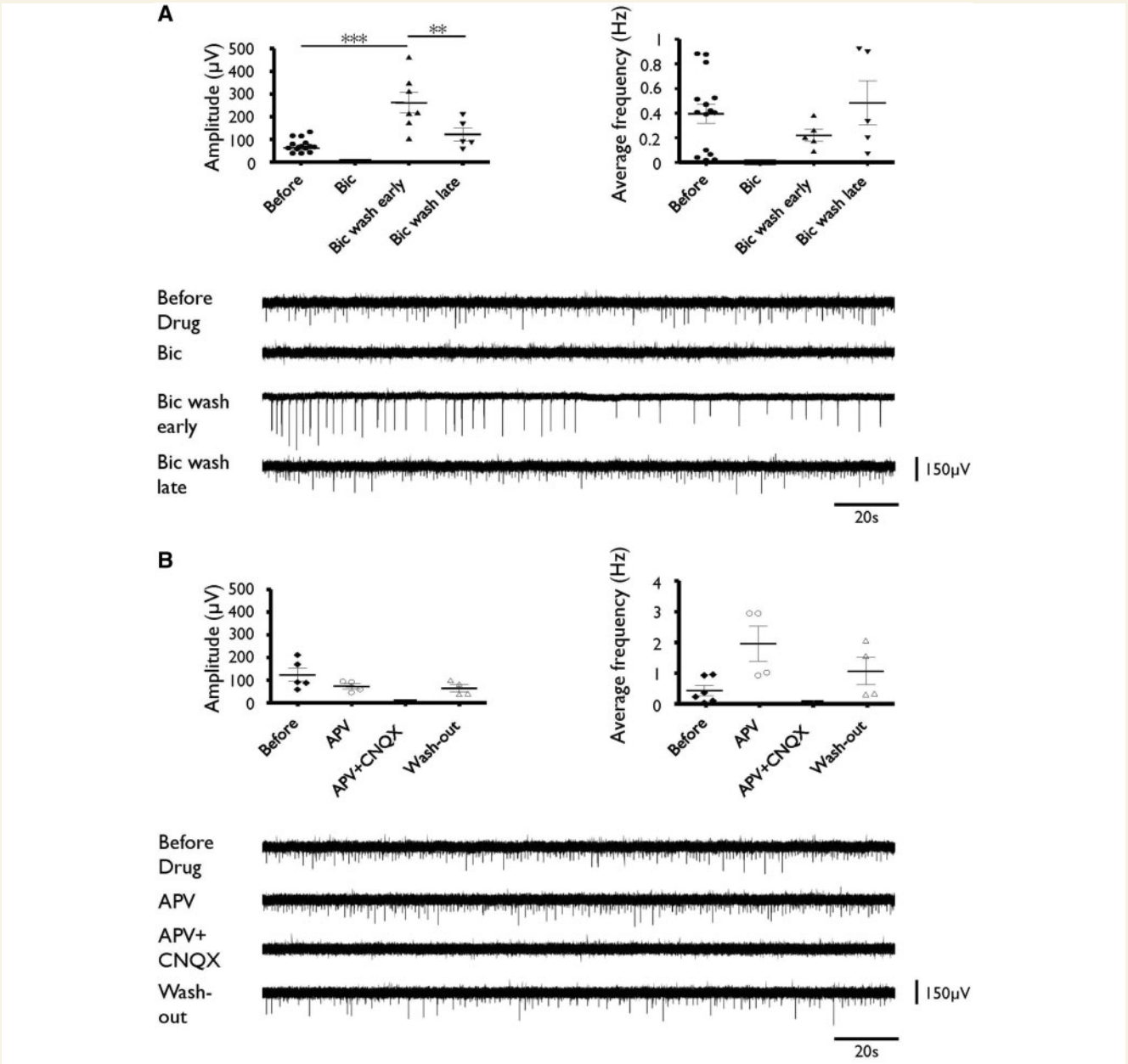

Figure 4 Basic pharmacological properties of interictal-like activity. (**A**) Effect of the $GABA_A$ receptor antagonist bicuculline (Bic, 10 μM). Panels display average amplitude (*left* histogram) and frequency (*right* histogram) of the interictal-like events before, during and after (early: ⩽16 min, late: >17 min) wash of Bic ($n = 8$ recording sites, from four slices derived from three patients). Original traces exemplify interictal-like activity before, during and after wash of Bic. (**B**) Effects of the glutamate receptor antagonists APV (50 μM) and CNQX (10 μM). Panels display average amplitude (*left* histogram) and frequency (*right* histogram) of the interictal-like events before, during and after application of APV and APV combined with CNQX ($n = 4$ recording sites, from two slices derived from two patients). Original traces exemplify interictal-like activity before, during and after wash of the glutamate receptor antagonists. $^{**}P < 0.01$; $^{***}P < 0.001$.

the 20 receptor binding sites tested and an overview of the results is provided in Table 3. Densities of glutamate AMPA ($P = 0.0000$), kainate ($P = 0.0000$) and mGluR2/3 ($P = 0.0000$), acetylcholine M_2 ($P = 0.0042$ when binding sites were visualized by means of the agonist oxotremorine-M; $P = 0.0081$ when binding sites were visualized by means of the antagonist AF-DX384) and noradrenalin α_1 ($P = 0.0023$) receptors were significantly increased in epileptic tissue. Conversely, densities of $GABA_A$ ($P = 0.0012$, when binding sites were visualized by means of the antagonist SR95531), acetylcholine M_3 ($P = 0.0006$) and serotonin 5-HT_{1A} ($P = 0.0400$) receptors were significantly downregulated in the lateral nucleus of epileptic cases. Interestingly, $GABA_A$ receptor density alterations were found to be significant when the receptor was labelled with the antagonist SR95531, but not with the agonist muscimol.

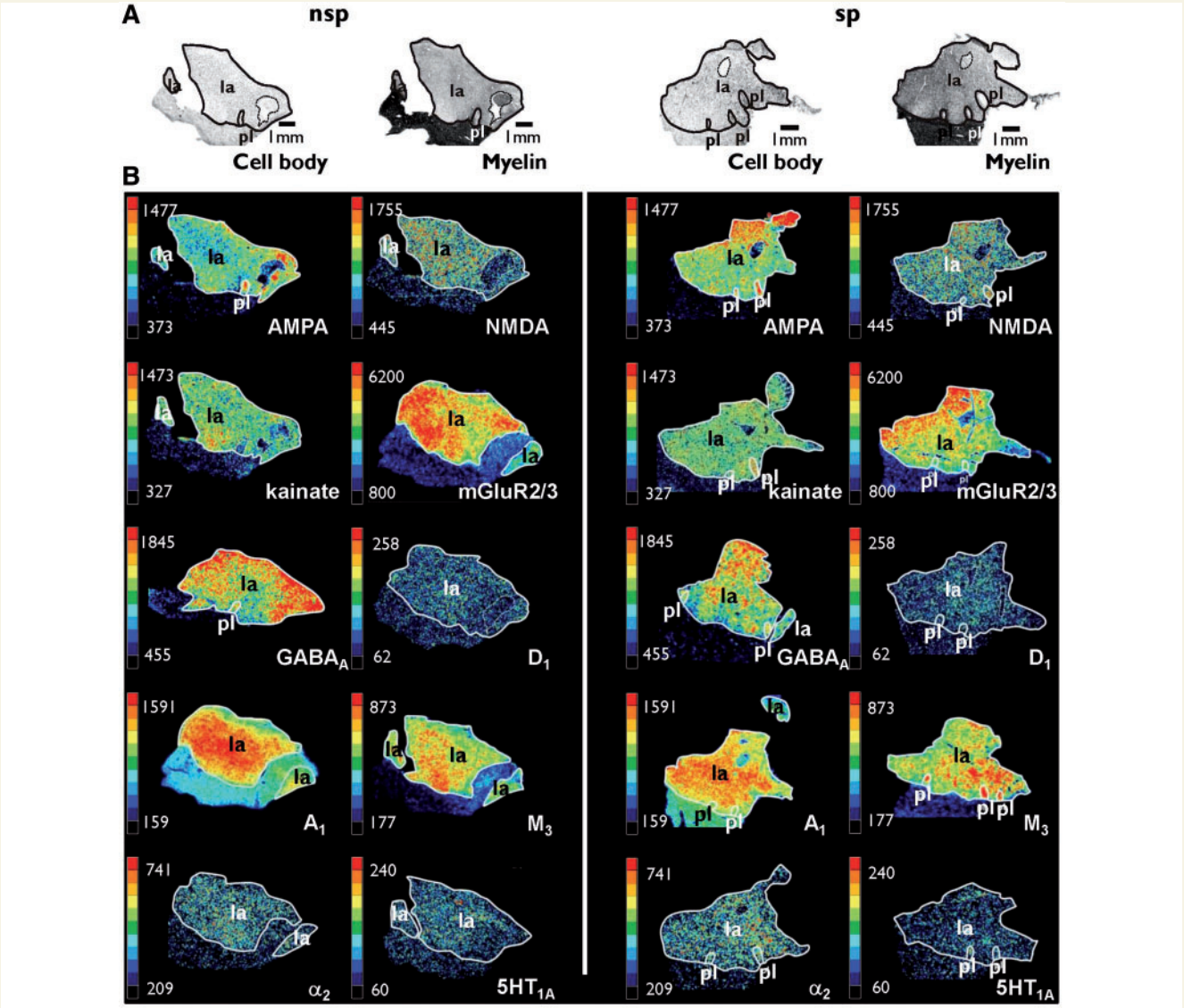

Figure 5 Examples of receptor autoradiographs from spontaneously (sp) and non-spontaneously (nsp) active slices. (**A**) Histological sections showing the cyto- and myeloarchitecture of parts of the amygdala in the region of the lateral nucleus. (**B**) Sections immediately neighbouring those shown in **A** were used for receptor autoradiography. Colour scales code receptor densities in fmol/mg protein for each receptor type. For this figure we chose sections labelled with [^{3}H]-AMPA to show AMPA receptors, [^{3}H]-MK 801 for NMDA receptors, [^{3}H]-Kainate for kainate receptors, [^{3}H]-LY 341 495 for mGlu2/3 receptors, [^{3}H]-muscimol for GABA$_A$ receptors, [^{3}H]-SCH 23390 for dopaminergic D$_1$ receptors, [^{3}H]-DPCPX for adenosine A$_1$ receptors, [^{3}H]-4 DAMP for muscarinic M$_3$ receptors, [^{3}H]-RX 821002 for noradrenergic α_2 receptors and [^{3}H]-8-OH-DPAT for serotonergic 5HT$_{1A}$ receptors. la = lateral nucleus; nsp = non-spontaneously active slices; pl = paralaminar nucleus; sp = spontaneously active slices.

Discussion

Amygdala tissue obtained from surgery of patients with medically intractable epilepsy provides an excellent opportunity to explore network properties of the human amygdala. This study focused on the lateral nucleus of the laterobasal group (Heimer *et al*., 1999), which displays synaptic organization and degenerative changes in human temporal lobe epilepsy (Aliaskevich *et al*., 2003; Yilmazer-Hanke *et al*., 2007). Here, we report that the human epileptic lateral nucleus can generate interictal activity and possesses? an expression profile of transmitter receptors that is different from that of controls.

Synaptic networks involved in generation of spontaneous interictal-like activity in the human lateral nucleus

The experimental approaches in the present study have been previously used to investigate properties of slices obtained from human neocortical tissue (Köhling *et al*., 1998, 2000).

Table 3 Binding site densities of neurotransmitter receptors (fmol/mg protein) and tritiated ligands used for labelling in the lateral nucleus of the amygdala in human epileptic ($n = 14$) and control slices ($n = 5$)

Neurotransmitter	Receptor	[^{3}H]-Ligand	Epilepsy		Control	
			Mean (SD)	SEM	Mean (SD)	SEM
Glutamate	AMPA	AMPA***	993 (91)	24	472 (123)	55
	kainate	Kainate***	1141 (136)	36	516 (282)	126
	NMDA	MK-801	1089 (184)	49	1164 (461)	206
	mGluR2/3	LY 341 495***	4613 (1161)	310	1670 (340)	152
GABA	$GABA_A$	Muscimol	1773 (387)	103	1518 (248)	111
		SR95531**	1636 (731)	195	2990 (427)	192
	$GABA_B$	CGP 54626	3599 (255)	68	3435 (558)	249
	BZ	Flumazenil	3033 (470)	126	3057 (375)	168
Acetylcholine	M_1	Pirenzepine	295 (136)	36	321 (144)	64
	M_2	Oxotremorine-M**	193 (60)	16	100 (31)	14
		AF-DX384**	367 (50)	13	287 (56)	25
	M_3	4-DAMP***	769 (121)	32	1036 (128)	57
	nACh	Epibatidine	77 (18)	5	61 (3)	2
Noradrenaline	α_1	Prazosin**	451 (76)	20	324 (33)	15
	α_2	UK 14 304	105 (30)	8	140 (49)	22
		RX 821 002	390 (80)	22	373 (99)	44
Serotonin	5-HT_{1A}	8-OH-DPAT*	91 (31)	8	131 (44)	20
	5-HT_2	Ketanserin	498 (118)	32	579 (53)	24
Dopamine	D_1	SCH 23 390	106 (17)	4	118 (53)	24
Adenosine	A_1	DPCPX	1338 (216)	58	1507 (374)	167

Asterisks indicate those binding sites for which significant ($P < 0.05$) differences were found between epileptic and control tissue.
*$P < 0.05$; **$P < 0.01$; ***$P < 0.001$.

Those studies reported spontaneous patterns of activity in the frontal neocortex resembling those found in the human lateral nucleus, and excluded the possibilities that this activity was artificially induced by the transport of the slices, raised levels of extracellular K^+ or washout of antiepileptic medication. Interestingly, a negative correlation was found between amygdala sclerosis and existence of interictal-like activity in lateral nucleus slices. Similar results have been obtained in the subiculum from epileptic patients (Cohen *et al*., 2002), suggesting that sclerosis in presumed input regions like the hippocampus results in alterations in target synaptic networks towards generation of spontaneous activity. In fact, hippocampal or rhinal cortical inputs are capable of synchronizing electrophysiological activity in the lateral nucleus in the 4-aminopyridine model in rodents (Klueva *et al*., 2003). In addition, intra-operative recordings obtained in patients of the present study show synchronous epileptic activity in both hippocampus and amygdala, whereas the cortex seems to have been spared.

Similar to interictal-like potentials recorded in various tissues obtained from epileptic patients (Köhling *et al*., 1998, 2000; Cohen *et al*., 2002; Huberfeld *et al*., 2007), the spontaneous events in the human lateral nucleus were sufficiently synchronous to support field potential discharges. Most human studies, however, have not found a predictable correlation between firing of single or populations of neurons and the interictal event (Wyler *et al*., 1982; Schwartzkroin *et al*., 1983). A recent study in epileptic patients suggested that interictal activity is not a simple paroxysm of hypersynchronous activity, but rather represents interplay of multiple neuronal types and local networks in functional 'microdomains' that can involve upregulation of both excitatory and inhibitory synaptic activity (Keller *et al*., 2010). In keeping with this, interictal-like events in the human lateral nucleus *in vitro* were typically initiated at various sites and did not necessarily appear synchronously across an entire slice. The existence of functional microdomains, heterogeneous neuronal populations and synaptic networks may also help to explain the finding that assessment of receptor densities across large territories in the lateral nucleus revealed no differences in receptor densities between spontaneously and non-spontaneously active tissue in the present study.

Receptor profiles in the human lateral nucleus related to epileptic activity

AMPA but not NMDA receptors seem to be critically involved in the generation of interictal-like activity in the human lateral nucleus (present study) and neocortex (Köhling *et al*., 1998). Slightly different conclusions have been reached in human hippocampal tissue, where spontaneous interictal-like activity was sensitive to a joint block of AMPA and NMDA receptors (Cohen *et al*., 2002). In the rat 4-aminopyridine model, AMPA receptors were indeed found to be involved in the recruitment of lateral nucleus projection neurons into interictal-like discharges of amygdala–entorhinal–perirhinal cortical networks *in vitro* (Klueva *et al*., 2003). The receptor profile of the human lateral nucleus indeed indicates a significant increase in AMPA receptor densities in the lateral nucleus of epileptic patients compared to autopsy controls, while there is no evidence for alterations of NMDA receptor densities.

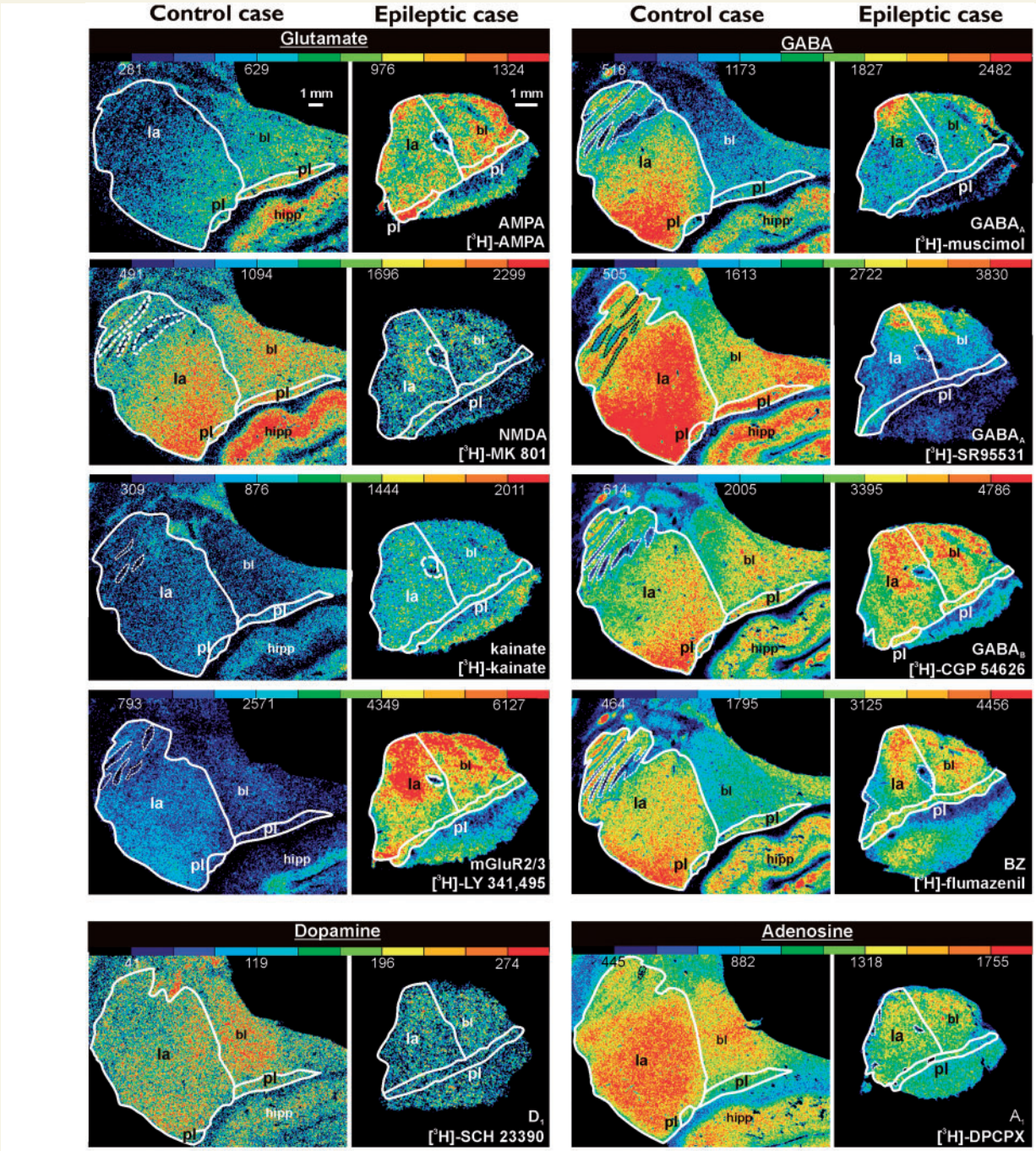

Figure 6 Receptor autoradiographs from control and epileptic tissue. Colour coded receptor autoradiographs of immediately neighbouring sections showing densities of the examined binding sites in control and epileptic tissue. All sections are from the same epileptic and control case. Sections have been matched in anterior-posterior direction. Colour scales code receptor densities in fmol/mg protein for each binding site type. $GABA_A$ receptors were visualized by means of the agonist [^{3}H]-muscimol and the antagonist [^{3}H]-SR95531. For further details concerning agonistic/antagonistic nature of ligands see Table 2. bl = basolateral nucleus; ec = entorhinal cortex; la = lateral nucleus; pl = paralaminar nucleus.

Of further note is the increase in kainate receptor densities in the epileptic human lateral nucleus. Since pharmacological approaches used in the present study do not allow us to discriminate between AMPA and kainate receptors (Honoré *et al.*, 1988), we cannot exclude the possibility that kainate receptors also participate in the generation of spontaneous interictal-like events. Kainate is indeed relevant to epileptic activity as demonstrated by the case study of a patient who developed *status epilepticus* followed by chronic temporal lobe epilepsy after intoxication by domoic acid, a kainate receptor agonist (Cendes *et al.*, 1995), and by the

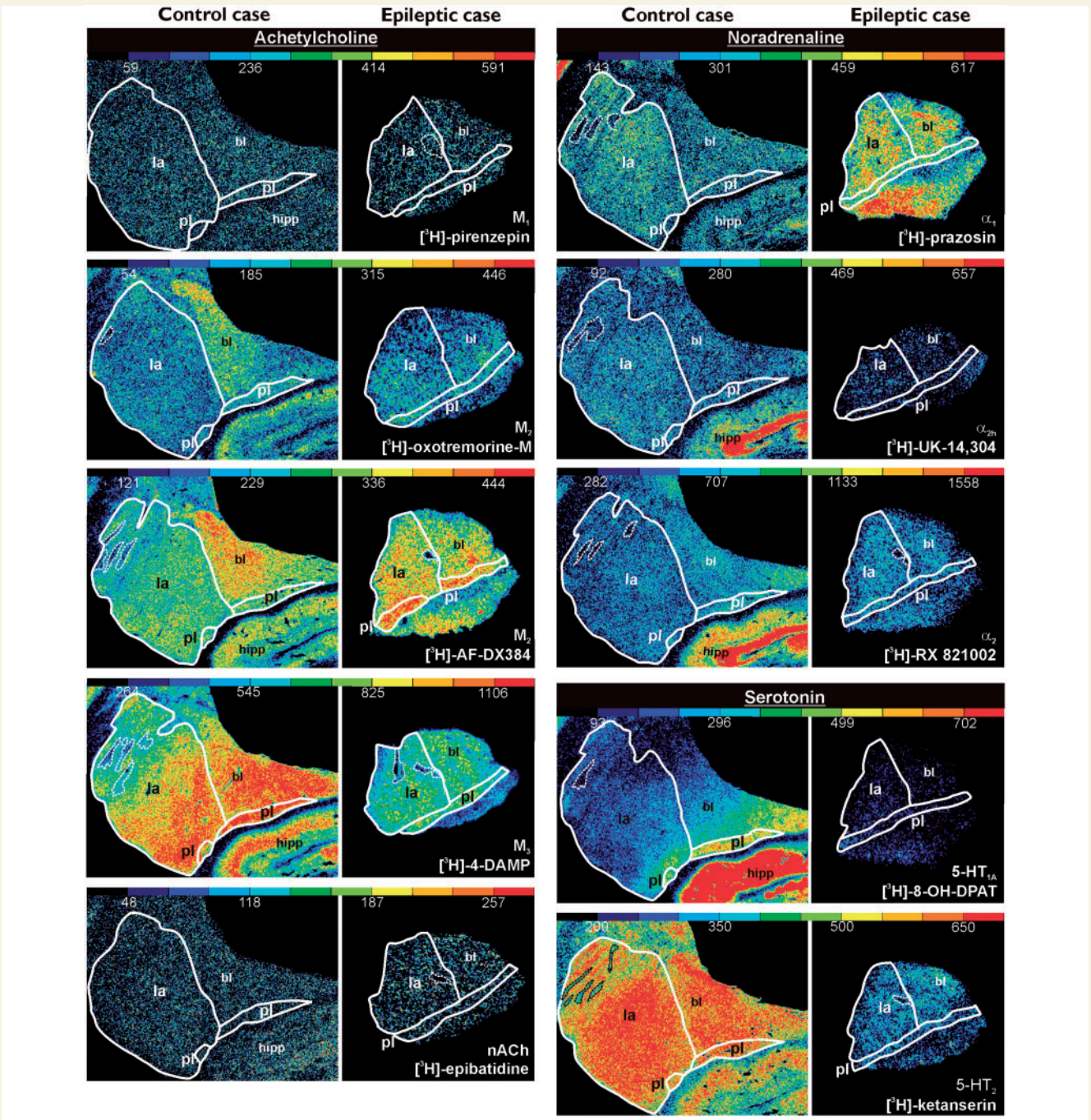

Figure 7 Receptor autoradiographs from control and epileptic tissue. Colour coded receptor autoradiographs of immediately neighbouring sections showing densities of the examined binding sites in control and epileptic tissue. Sections have been matched in an anterior-posterior direction. Same cases as in Fig. 6. Colour scales code receptor densities in fmol/mg protein for each binding site type. Muscarinic cholinergic M_2 receptors were visualized by means of the agonist [^{3}H]-oxotremorine-M and the antagonist [^{3}H]-AF-DX384. For further details concerning agonistic/antagonistic nature of ligands see Table 2. bl = basolateral nucleus; ec = entorhinal cortex; hipp = hippocampus; la = lateral nucleus; pl = paralaminar nucleus.

common use of kainate to produce rodent models of temporal lobe epilepsy (Morimoto *et al*., 2004).

Of particular importance in the understanding of the origin of spontaneous activity is the notion that concerted firing of a subset of inhibitory interneurons may critically contribute to the initiation of the interictal spike component by mediating an initial period of inhibition followed by a hyper-synchronous excitatory rebound (Keller *et al*., 2010). While analyses on the single neuron level have not been attempted in the present study, it is interesting to note that application of the $GABA_A$ receptor antagonist

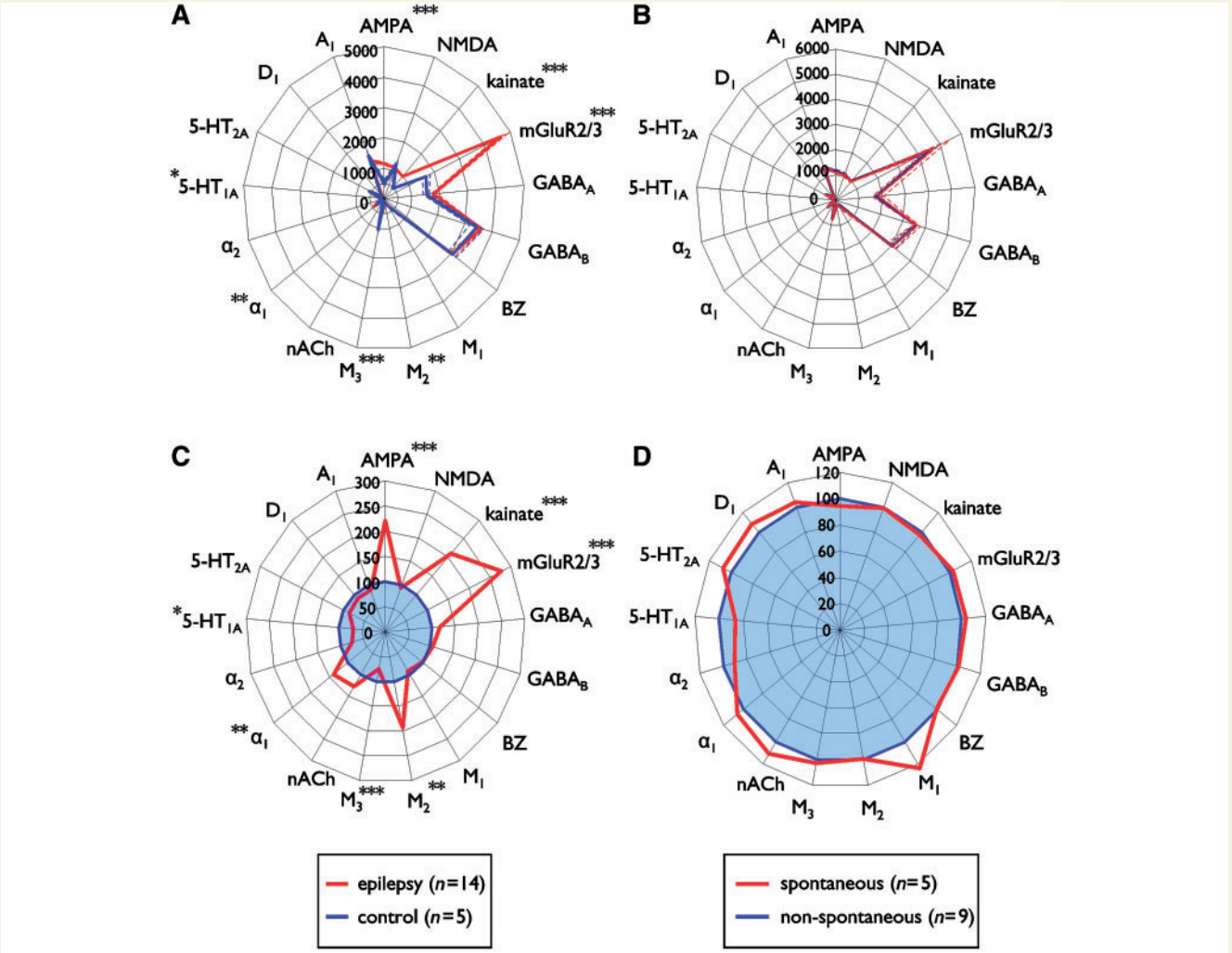

Figure 8 Receptor fingerprints. (**A**) Polar plots representing absolute binding site concentrations in epileptic (red traces, $n = 14$ slices derived from nine patients) versus control (blue traces, $n = 5$ slices derived from five patients) cases (Fig. 7A) and (**B**) in spontaneous (red traces) versus non-spontaneous (blue traces) tissue (Fig. 7B). (**C**) Polar plots representing the normalized binding site concentrations in the epileptic (red traces) tissue as a ratio of that in the control (blue traces) tissue (Fig. 7C), and in (**D**) the spontaneous (red traces) tissue as a ratio of that in the non-spontaneous (blue traces) tissue (Fig. 7D). $*P < 0.05$; $**P < 0.01$; $***P < 0.001$. α_1 and α_2 (labelled with [^{3}H]-UK 14,304) = noradrenergic receptors; 5-HT$_{1A}$ and 5-HT$_2$ = serotonergic receptors; A$_1$ = adenosine receptor; AMPA = glutamatergic AMPA receptor; BZ = benzodiazepine binding site of the GABA$_A$ receptor; GABA$_A$ = GABA$_A$ receptor (labelled with [^{3}H]-muscimol); GABA$_B$ = GABA$_B$ receptor; Kainate = glutamatergic kainate receptor; M_1, M_2 (labelled with [^{3}H]-oxotremorine-M) and M_3 = cholinergic muscarinic receptors; mGluR2/3 = metabotropic glutamatergic receptor; nACh = cholinergic nicotinic receptor; NMDA = glutamatergic NMDA receptor.

bicuculline resulted in a blockade of spontaneous interictal-like activity in the human lateral nucleus, and a rebound effect with increased amplitude of the activity upon washout, supporting the notion of a critical contribution of GABAergic synaptic mechanisms. Abnormalities in GABA receptor function and synaptic connectivity rather than a full block of GABAergic influences across large territories have been previously reported to occur in various human epileptic tissues, including the lateral nucleus (Huberfeld *et al*., 2007; Sen *et al*., 2007; Yilmazer-Hanke *et al*., 2007). More specifically, a reduction of GABA-containing axo-somatic synaptic contacts on putative projection neurons has been found in the lateral nucleus from patients with epilepsy compared with autopsy controls (Aliashkevich *et al*., 2003), which was inversely correlated with the extent of fibrillary gliosis (Yilmazer-Hanke et al., 2007). Regarding GABAergic transmission, a decreased binding of the GABA$_A$ receptor antagonist SR95531 was indeed observed in the epileptic lateral nucleus as compared with control lateral nucleus in the present study, while no such difference was evident for the GABA$_A$ receptor agonist muscimol. Considering that agonists bind with a higher affinity to the active form of the receptor than to the inactive form, whereas antagonists do not discriminate between active or inactive receptor states (Leff, 1995), the present data thus suggest a reduction in the overall number of GABA$_A$ receptors in the epileptic lateral nucleus.

From those data, it seems feasible to conclude that an altered balance between excitatory and inhibitory neurotransmission, involving an increase in AMPA and/or kainate and a decrease in $GABA_A$ binding site densities in synaptic networks and/or synaptic contacts between GABAergic and projection neurons, is critical for generation of epileptic activity in the lateral nucleus.

Receptor autoradiography analysis in addition demonstrates that receptor densities of cholinergic, adrenergic and serotonergic transmitter systems are altered in the epileptic lateral nucleus. The cholinergic system plays an important role in seizure control and development, as indicated for instance by the common use of the antiepileptic drug lamotrigin, a drug acting through blockade of nicotinic cholinergic receptors (Zheng *et al.*, 2010), and by the progressive development of spontaneously recurrent seizures in the pilocarpine model of temporal lobe epilepsy, a model that uses a muscarinic blocker to induce an initial *status epilepticus*. Although we found no significant changes of nicotinic receptors, the density of M_2 and M_3 muscarinic receptors were significantly altered in the epileptic tissue as compared with controls. Regarding the serotonergic system, the present study reports on a downregulation of 5-HT_{1A} receptors, which probably results in a facilitation of seizure maintenance, in accordance with the antiepileptogenic nature of serotonin (Bagdy *et al.*, 2007). The observed upregulation of the α_1 adrenoceptor in the epileptic lateral nucleus are difficult to interpret, since both pro- and anticonvulsant effects have been associated with this receptor type. For example, α_1 receptor activation was shown to potentiate glutamate- or acetylcholine-evoked excitatory discharges (Mouradian *et al.*, 1991) and mice over-expressing the α_{1B} receptor exhibit spontaneous interictal epileptic spikes and seizures (Kunieda *et al.*, 2002). On the other hand, an α_1 receptor antagonist was shown to act as a proconvulsant in a case study of a patient with medial temporal lobe seizures (Ivanez and Ojeda, 2006), and application of the α_1 receptor agonist St 587 had an anti-convulsant effect in kindled rats and epileptic gerbils (Löscher and Czuczwar, 1987). The decreased density of serotonin receptors of type 1A, perhaps as a consequence of seizure activity, likely results in a decrease in hyperpolarizing influence thereby a contribution to hyperexcitability (for review see Bagdy *et al.*, 2007). Finally, an increase in receptor densities of mGluR2/3 could represent compensatory mechanisms globally aiming at reducing excitability (Bymaster *et al.* 2003; Scorza et al. 2009).

Together these data indicate an abnormal pattern of receptor densities and synaptic function in the lateral nucleus of the amygdala in epileptic patients, which may give rise to domains of spontaneous interictal-like discharges contributing to seizure activity in the amygdala. Future studies are needed to relate these abnormalities to defined receptor subunits, types of neurons and synaptic interconnections, and to identify the mechanisms leading to epileptic seizures in larger territories of the amygdaloid and connected networks. Importantly, these studies will also need to clarify the possible influence of maintained epileptic activity on patterns of receptor expression, alterations of which may act as a homeostatic protective mechanism (Ben-Ari *et al.*, 2008).

Acknowledgements

We would like to thank Birgit Herrenpoth, Patrick Meuth (assistance with computer programming), Markus Cremer (receptor autoradiography), Stephanie Krause (histology), Jessica Bausch and Sabrina Buller (digital processing of receptor autoradiographs) for excellent technical assistance.

Funding

Deutsche Forschungsgemeinschaft (DFG; SFB-TR3, TP C3; to H.C.P. and E.J.S.); a research award (Max-Planck-Research Award 2007; to H.C.P.); the Helmholtz Alliances HelMA (Health in an Aging Society, to K.Z.); Systems Biology (to K.Z.).

References

Aliashkevich AF, Yilmazer-Hanke D, Van Roost D, Mundhenk B, Schramm J, Blumcke I. Cellular pathology of amygdala neurons in human temporal lobe epilepsy. Acta Neuropathol 2003; 106: 99–106.

Avoli M, D'Antuono M, Louvel J, Köhling R, Biagini G, Pumain R, et al. Network and pharmacological mechanisms leading to epileptiform synchronization in the limbic system in vitro. Prog Neurobiol 2002; 68: 167–207.

Bagdy G, Kecskemeti V, Riba P, Jakus R. Serotonin and epilepsy. J Neurochem 2007; 100: 857–73.

Benini R, Avoli M. Altered inhibition in lateral amygdala networks in a rat model of temporal lobe epilepsy. J Neurophysiol 2006; 95: 2143–54.

Ben-Ari Y, Crepel V, Represa A. Seizures beget seizures in temporal lobe epilepsies: the boomerang effects of newly formed aberrant kainatergic synapses. Epilepsy Curr 2008; 8: 68–72.

Biraben A, Taussig D, Thomas P, Even C, Vignal JP, Scarabin JM, et al. Fear as the main feature of epileptic seizures. J Neurol Neurosurg Psychiatry 2001; 70: 186–91.

Bymaster FP, McKinzie DL, Felder CC, Wess J. Use of M_1-M_5 muscarinic receptor knockout mice as novel tools to delineate the physiological roles of the muscarinic cholinergic system. Neurochem Res 2003; 28: 437–42.

Cendes F, Andermann F, Carpenter S, Zatorre RJ, Cashman NR. Temporal lobe epilepsy caused by domoic acid intoxication: evidence for glutamate receptor-mediated excitotoxicity in humans. Ann Neurol 1995; 37: 123–6.

Cendes F, Andermann F, Gloor P, Gambardella A, Lopes-Cendes I, Watson C, et al. Relationship between atrophy of the amygdala and ictal fear in temporal lobe epilepsy. Brain 1994; 117: 739–46.

Cohen I, Navarro V, Clemenceau S, Baulac M, Miles R. On the origin of interictal activity in human temporal lobe epilepsy in vitro. Science 2002; 298: 1418–21.

Cremer CM, Palomero-Gallagher N, Bidmon HJ, Schleicher A, Speckmann EJ, Zilles K. Pentylenetetrazole-induced seizures affect binding site densities for GABA, glutamate and adenosine receptors in the rat brain. Neuroscience 2009; 163: 490–9.

de Olmos JS. The amygdala in the human nervous system. San Diego: Elsevier; 2004.

Engel J Jr, Pedley TA, Aicardi J, Dichter MA, Moshé S. Epilepsy: a comprehensive textbook. 2nd edn. Philadelphia, PA: Lippincott Williams & Wilki; 2007.

Gallyas F. Silver staining of myelin by means of physical development. Neurol Res 1979; 1: 203–9.

Gilby KL, Da Silva AG, McIntyre DC. Differential $GABA_A$ subunit expression following status epilepticus in seizure-prone and seizure-resistant rats: a putative mechanism for refractory drug response. Epilepsia 2005; 46: 3–9.

Giovacchini G, Toczek MT, Bonwetsch R, Bagic A, Lang L, Fraser C, et al. 5-HT_{1A} receptors are reduced in temporal lobe epilepsy after partial-volume correction. J Nucl Med 2005; 46: 1128–35.

Gloor P. Role of the amygdala in temporal lobe epilepsy. The amygdala: Neurobiological aspects of emotion, memory, and mental dysfunction. Wiley-Liss, Inc.; 1992. p. 505–38.

Graebenitz S, Lesting J, Sosulina L, Seidenbecher T, Pape HC. Alteration of NMDA receptor-mediated synaptic interactions in the lateral amygdala associated with seizure activity in a mouse model of chronic temporal lobe epilepsy. Epilepsia 2010; 51: 1754–62.

Heimer L, de Olmos JS, Alheid GF, Pearson J, Sakamoto N, Shinoda K, et al. The human basal forebrain. Part II. The primate nervous system, Part III. Elsevier; 1999. p. 57–226.

Honoré T, Davies SN, Drejer J, Fletcher EJ, Jacobsen P, Lodge D, et al. Quinoxalinediones: potent competitive non-NMDA glutamate receptor antagonists. Science 1988; 241: 701–3.

Huberfeld G, Wittner L, Clemenceau S, Baulac M, Kaila K, Miles R, et al. Perturbed chloride homeostasis and GABAergic signaling in human temporal lobe epilepsy. J Neurosci 2007; 27: 9866–73.

Hufnagel A, Dumpelmann M, Zentner J, Schijns O, Elger CE. Clinical relevance of quantified intracranial interictal spike activity in presurgical evaluation of epilepsy. Epilepsia 2000; 41: 467–78.

Hüttmann K, Yilmazer-Hanke D, Seifert G, Schramm J, Pape HC, Steinhauser C. Molecular and functional properties of neurons in the human lateral amygdala. Mol Cell Neurosci 2006; 31: 210–7.

Ivanez V, Ojeda J. Exacerbation of seizures in medial temporal lobe epilepsy due to an alpha1-adrenergic antagonist. Epilepsia 2006; 47: 1741–2.

Keller CJ, Truccolo W, Gale JT, Eskandar E, Thesen T, Carlson C, et al. Heterogeneous neuronal firing patterns during interictal epileptiform discharges in the human cortex. Brain 2010; 133: 1668–81.

Klueva J, Munsch T, Albrecht D, Pape HC. Synaptic and non-synaptic mechanisms of amygdala recruitment into temporolimbic epileptiform activities. Eur J Neurosci 2003; 18: 2779–91.

Koch UR, Musshoff U, Pannek HW, Ebner A, Wolf P, Speckmann EJ, et al. Intrinsic excitability, synaptic potentials, and short-term plasticity in human epileptic neocortex. J Neurosci Res 2005; 80: 715–26.

Köhling R, Lücke A, Straub H, Speckmann EJ. A portable chamber for long-distance transport of surviving human brain slice preparations. J Neurosci Methods 1996; 67: 233–6.

Köhling R, Hohling JM, Straub H, Kuhlmann D, Kuhnt U, Tuxhorn I, et al. Optical monitoring of neuronal activity during spontaneous sharp waves in chronically epileptic human neocortical tissue. J Neurophysiol 2000; 84: 2161–5.

Köhling R, Lücke A, Straub H, Speckmann EJ, Tuxhorn I, Wolf P, et al. Spontaneous sharp waves in human neocortical slices excised from epileptic patients. Brain 1998; 121: 1073–87.

Kral T, Clusmann H, Urbach J, Schramm J, Elger CE, Kurthen M, et al. Preoperative evaluation for epilepsy surgery (Bonn Algorithm). Zentralbl Neurochir 2002; 63: 106–10.

Kunieda T, Zuscik MJ, Boongird A, Perez DM, Luders HO, Najm IM. Systemic overexpression of the α_{1B}-adrenergic receptor in mice: an animal model of epilepsy. Epilepsia 2002; 43: 1324–9.

LeDoux JE. Emotion circuits in the brain. Annu Rev Neurosci 2000; 23: 155–84.

Lee S, Miskovsky J, Williamson J, Howells R, Devinsky O, Lothman E, et al. Changes in glutamate receptor and proenkephalin gene expression after kindled seizures. Brain Res Mol Brain Res 1994; 24: 34–42.

Leff P. The two-state model of receptor activation. Trends Pharmacol Sci 1995; 16: 89–97.

Löscher W, Czuczwar SJ. Comparison of drugs with different selectivity for central alpha 1- and alpha 2-adrenoceptors in animal models of epilepsy. Epilepsy Res 1987; 1: 165–72.

Merker B. Silver staining of cell bodies by means of physical development. J Neurosci Methods 1983; 9: 235–41.

Morimoto K, Fahnestock M, Racine RJ. Kindling and status epilepticus models of epilepsy: rewiring the brain. Prog Neurobiol 2004; 73: 1–60.

Mouradian RD, Sessler FM, Waterhouse BD. Noradrenergic potentiation of excitatory transmitter action in cerebrocortical slices: evidence for mediation by an α_1 receptor-linked second messenger pathway. Brain Res 1991; 546: 83–95.

Palomero-Gallagher N, Vogt BA, Schleicher A, Mayberg HS, Zilles K. Receptor architecture of human cingulate cortex: evaluation of the four-region neurobiological model. Hum Brain Mapp 2009; 30: 2336–55.

Pitkänen A, Pikkarainen M, Nurminen N, Ylinen A. Reciprocal connections between the amygdala and the hippocampal formation, perirhinal cortex, and postrhinal cortex in rat. A review. Ann N Y Acad Sci 2000; 911: 369–91.

Pitkänen A, Tuunanen J, Kälviäinen R, Partanen K, Salmenperä T. Amygdala damage in experimental and human temporal lobe epilepsy. Epilepsy Res 1998; 32: 233–53.

Prince HK, Conn PJ, Blackstone CD, Huganir RL, Levey AI. Down-regulation of AMPA receptor subunit GluR2 in amygdaloid kindling. J Neurochem 1995; 64: 462–5.

Quesney LF. Clinical and EEG features of complex partial seizures of temporal lobe origin. Epilepsia 1986; 27 (Suppl 2): 27–45.

Savic I, Lindström P, Gulyás B, Halldin C, Andrée B, Farde L. Limbic reductions of 5-HT_{1A} receptor binding in human temporal lobe epilepsy. Neurology 2004; 62: 1343–51.

Schliebs R, Zivin M, Steinbach J, Rothe T. Changes in cholinergic but not in GABAergic markers in amygdala, piriform cortex, and nucleus basalis of the rat brain following systemic administration of kainic acid. J Neurochem 1989; 53: 212–8.

Schwartzkroin PA, Turner DA, Knowles WD, Wyler AR. Studies of human and monkey "epileptic" neocortex in the in vitro slice preparation. Ann Neurol 1983; 13: 249–57.

Scorza FA, Arida RM, Naffah-Mazzacoratti MG, Scerni DA, Calderazzo L, Cavalheiro EA. The pilocarpine model of epilepsy: what have we learned? An Acad Bras Cienc 2009; 81: 345–65.

Sen A, Martinian L, Nikolic M, Walker MC, Thom M, Sisodiya SM. Increased NKCC1 expression in refractory human epilepsy. Epilepsy Res 2007; 74: 220–7.

Shoji Y, Tanaka E, Yamamoto S, Maeda H, Higashi H. Mechanisms underlying the enhancement of excitatory synaptic transmission in basolateral amygdala neurons of the kindling rat. J Neurophysiol 1998; 80: 638–46.

Sloviter RS. Hippocampal pathology and pathophysiology in temporal lobe epilepsy. Neurologia 1996; 11 (Suppl 4): 29–32.

Tuunanen J, Halonen T, Pitkänen A. Status epilepticus causes selective regional damage and loss of GABAergic neurons in the rat amygdaloid complex. Eur J Neurosci 1996; 8: 2711–25.

Watson J, Collin L, Ho M, Riley G, Scott C, Selkirk JV, et al. 5-HT_{1A} receptor agonist-antagonist binding affinity difference as a measure of intrinsic activity in recombinant and native tissue systems. Brit J Pharmacol 2000; 130: 1108–14.

Wyler AR, Ojemann GA, Ward AA Jr. Neurons in human epileptic cortex: correlation between unit and EEG activity. Ann Neurol 1982; 11: 301–8.

Wyler AR, Curtis Dohan JrF, Schweitzer JB, Berry AD III. A grading system for mesial temporal pathology (hippocampal sclerosis) from anterior temporal lobectomy. J Epilepsy 1992; 5: 220–5.

Yilmazer-Hanke DM, Wolf HK, Schramm J, Elger CE, Wiestler OD, Blumcke I. Subregional pathology of the amygdala complex and entorhinal region in surgical specimens from patients with pharmacoresistant temporal lobe epilepsy. J Neuropathol Exp Neurol 2000; 59: 907–20.

Yilmazer-Hanke DM, Faber-Zuschratter H, Blümcke I, Bickel M, Becker A, Mawrin C, et al. Axo-somatic inhibition of projection neurons in the lateral nucleus of amygdala in human temporal lobe epilepsy: an ultrastructural study. Exp Brain Res 2007; 177: 384–99.

Zheng C, Yang K, Liu Q, Wang MY, Shen J, Valles AS, et al. The anticonvulsive drug lamotrigine blocks neuronal {alpha}4{beta}2 nicotinic acetylcholine receptors. J Pharmacol Exp Ther 2010; 335: 401–8.

Zilles K, Qü MS, Köhling R, Speckmann EJ. Ionotropic glutamate and GABA receptors in human epileptic neocortical tissue: quantitative in vitro receptor autoradiography. Neuroscience 1999; 94: 1051–61.

Zilles K, Schleicher A, Palomero-Gallagher N, Amunts K. Quantitative analysis of cyto- and receptor architecture of the human brain. In: Toga AW, Mazziotta JC, editors. Brain mapping. The methods. Amsterdam: Elsevier; 2002a. p. 573–602.

Zilles K, Palomero-Gallagher N, Grefkes C, Scheperjans F, Boy C, Amunts K, et al. Architectonics of the human cerebral cortex and transmitter receptor fingerprints: reconciling functional neuroanatomy and neurochemistry. Eur Neuropsychopharmacol 2002b; 12: 587–99.